

Fluorine Abundances in Local Stellar Populations

K. E. BRADY,¹ C. A. PILACHOWSKI,¹ V. GRISONI,² Z. G. MAAS,¹ AND K. A. NAULT³

¹*Indiana University Bloomington, Department of Astronomy, 727 East 3rd St., Bloomington, IN 47405, USA*

²*INAF, Osservatorio Astronomico di Trieste, via G.B. Tiepolo 11, I-34131, Trieste, Italy*

³*University of Iowa, Department of Physics and Astronomy, 203 Van Allen Hall, Iowa City, IA 52242, USA*

ABSTRACT

We present the first fluorine measurements in 12 normal giants belonging to the Galactic thin and thick disks using spectra obtained with the Phoenix infrared spectrometer on the 2.1m telescope at Kitt Peak. Abundances are determined from the (1–0) R9 2.3358 μm feature of the molecule HF. Additionally, sodium abundances are derived in 25 giants in the thin disk, thick disk, and halo using the Na I line at 2.3379 μm . We report fluorine abundances for thin and thick disk stars in the metallicity range $-0.7 < [\text{Fe}/\text{H}] < 0$. We add two abundance measurements for stars with $[\text{Fe}/\text{H}] < 0.5$ dex which are at a critical metallicity range to constrain models. We find a larger dispersion in fluorine abundances than sodium abundances despite both species having similar overall uncertainties due to atmospheric parameters, suggesting this dispersion is real and not observational. The dispersion is slightly larger in the thick disk than the thin. The thin and thick disk average $[\text{F}/\text{Fe}]$ for our sample of stars combined with the literature differ by 0.03 dex. The observations are compared to available chemical evolution models.

Keywords: Stars: Abundances, Stars: Late Type; Galaxy: abundances; Galaxy: disk

1. INTRODUCTION

The abundances of light elements provide insight into the chemical evolution of the Milky Way and its stellar populations (see [Matteucci 2021](#) for a review). The cosmic origin of light elements with even atomic numbers (e.g., O, Mg, Si) is generally well understood, but the origin of many odd- Z elements (e.g., F, P, Cl) remains under debate ([Nomoto et al. 2013](#)). Understanding the formation of odd elements provides an opportunity to constrain nucleosynthesis processes as, for example, ^{19}F (the lone stable isotope of fluorine) is integral in proton-capture reactions that include the CNO and Ne–Na cycles.

The light, odd- Z element fluorine is thought to be produced in multiple stellar sites such as asymptotic giant branch (AGB) stars ([Jorissen et al. 1992](#)), rapidly rotating massive stars ([Prantzos et al. 2018](#)), Wolf–Rayet stars ([Meynet & Arnould 2000](#)), the ν process in core-collapse supernovae ([Woosley & Haxton 1988](#)), and novae ([Olive & Vangioni 2019](#)). In the context of Galactic chemical evolution, several nucleosynthetic channels may contribute to the Galactic fluorine abundance, with different processes dominating certain stellar populations (such as thin-disk, thick-disk, and bulge stars) and/or at certain metallicities. For a comprehensive re-

view of the proposed nucleosynthetic sources of fluorine, see Section 5.1 in [Ryde et al. \(2020\)](#).

Determining the abundance of fluorine in stars remains difficult due to many observational challenges. Due to the lack of strong, measurable atomic fluorine lines, the only indicator of fluorine abundance that can be measured in cool atmospheres are spectral lines from the hydrogen fluoride (HF) molecule. Vibration-rotation HF lines exist in the K band, and pure rotational HF lines in the N band. Telluric lines in the near-infrared (near-IR) can complicate the derivation of abundances, and the HF molecule has a relatively low dissociation energy, limiting studies to stars below ~ 4700 K.

While early work on the abundance of fluorine in stars focused primarily on AGB stars (e.g., [Jorissen et al. 1992](#); [Cunha et al. 2000](#); [Abia et al. 2009, 2010](#)) and carbon-enhanced metal-poor stars ([Schuler et al. 2007](#); [Lucatello et al. 2011](#)), recent investigations have turned to the determination of the fluorine abundance in main-sequence and pre-AGB giant stars to identify the source of fluorine in the Milky Way. These studies, such as [Jönsson et al. \(2014a, 2017\)](#), [Pilachowski & Pace \(2015\)](#), [Guerço et al. \(2019\)](#), and [Ryde et al. \(2020\)](#), use high-resolution spectrometers in the near-IR to measure HF

at $2.3 \mu\text{m}$. For the first time in abundance derivation studies, Jönsson et al. (2014b) explored a pure rotational HF line at $12.2 \mu\text{m}$, finding that the derived fluorine abundance agreed with the $2.3 \mu\text{m}$ vibrational-rotational HF line. Many of these studies have contrasting conclusions regarding the chemical evolution of fluorine in the Milky Way. Most recently, Ryde et al. (2020) indicated a need for multiple cosmic sources of fluorine over time.

The solar abundance of fluorine was originally determined to be $\log \epsilon(\text{F}) = 4.56 \pm 0.30$ by Hall & Noyes (1969) based on observations of sunspots. Since then, new measurements of the oscillator strengths and excitation potentials of the IR (1–0) HF features have become available in the HITRAN database (Rothman et al. 2013), and Maiorca et al. (2014) have reanalyzed the solar abundance of fluorine. With the new, experimental molecular data, Maiorca et al. (2014) found a solar fluorine abundance of $\log \epsilon(\text{F}) = 4.40 \pm 0.25$ from a careful analysis of eight HF features in sunspot umbral spectra from the Wallace et al. (2001) atlas. This value is in good agreement with the meteoritic abundance at $\log \epsilon(\text{F}) = 4.42 \pm 0.06$ (Lodders et al. 2009).

Just as new observational results became available, so too have new chemical-enrichment models that provide a theoretical framework for interpreting the abundance of fluorine in the Galactic disk. Authors include different nucleosynthesis prescriptions for fluorine to predict the abundance of fluorine as a function of $[\text{Fe}/\text{H}]^1$ and $[\text{O}/\text{H}]$. Recent studies include Kobayashi et al. (2011a, 2020), Spitoni et al. (2018), Prantzos et al. (2018), Olive & Vangioni (2019), Grisoni et al. (2020), and Womack et al. (2023).

In this work, we report on new determinations of the abundance of fluorine in giants belonging to the Galactic thin and thick disks, and compare the dependence of $[\text{F}/\text{Fe}]$ on $[\text{Fe}/\text{H}]$ and $[\text{F}/\text{O}]$ on $[\text{O}/\text{H}]$ both with the thin and thick disks and with theoretical models. In Section §2 we describe the target selection, observations, and data reduction. Section §3 details the spectral analysis. We compare our results to the literature in Section §4. In Sections §5 and §6 we discuss fluorine enrichment in the thin and thick disks and the chemical evolution of fluorine. Finally, in Section §7 we summarize our results.

2. OBSERVATIONS AND DATA REDUCTION

2.1. Target Selection

Candidate stars belonging to the Galactic disk were selected for observation from the surveys of Barbuy & Erdelyo-Mendes (1989), McWilliam (1990), Alves-Brito et al. (2010), Ramírez et al. (2013), Prugniel et al. (2011), Wu et al. (2011), and Pakhomov (2013). UVW space velocities were computed using the PyAstronomy Galactic space velocity function² with the peculiar solar motion correction from Ding et al. (2019). Coordinates, proper motions, distances, and radial velocities were taken from the Gaia Data Release 3 (DR3; Gaia Collaboration et al. 2016, 2023). Membership in different kinematic groups was established by requiring that the probability of belonging to one population be greater than 50%, following the methodology of Johnson & Soderblom (1987) as described by Ramírez et al. (2013). The final sample includes nine thin-disk stars, sixteen thick-disk stars, and two halo stars, as shown in Table 1.

2.2. Observations

Spectra covering the relatively unblended $2.3359 \mu\text{m}$ (1–0) R9 feature of HF and the Na I line at $2.3379 \mu\text{m}$ were obtained using the Phoenix infrared spectrometer on the 2.1m telescope at the Kitt Peak National Observatory in 2012 November and December, and 2013 December. The spectrometer was configured with a $0.7''$ slit and the 4308 filter to isolate grating order 32, providing spectral coverage from 2.3285 to $2.3390 \mu\text{m}$. Observations were obtained at two slit positions for subtraction of a simultaneous sky spectrum and dark current. Hot stars were observed frequently on each night at similar air mass to allow effective telluric-line correction, and stars were observed close to the meridian to minimize telluric absorption features.

2.3. Data Reduction

Spectra were reduced by subtracting background and night-sky emission using the ABBA observing technique, correcting for variations in pixel sensitivity by dividing by a continuous lamp spectrum, extracting one-dimensional spectra, removing telluric-line contamination by dividing by the spectrum of a hot star, and calibrating the wavelength scale using telluric methane lines in the hot-star spectra. Finally, the spectra were normalized in the continuum and shifted to match the laboratory rest wavelength scale. The observations of each star, including star identifications, spectral types and K magnitudes from SIMBAD, the dates of observation, the

¹ We use the standard spectroscopic notation where $[A/B] \equiv \log(N_A/N_B)_{\text{star}} - \log(N_A/N_B)_{\odot}$ and $\log \epsilon(A) \equiv \log(N_A/N_H) + 12.0$ for elements A and B.

² https://pyastronomy.readthedocs.io/en/latest/pyaslDoc/aslDoc/gal_uvw.html

Table 1. Stars Observed with Phoenix and the Kitt Peak 2.1 m Telescope

Star	HIP	Alt.	Spec. Type	K Mag.	UT Date	Exp. Time (s)	S/N Ratio
Thin Disk							
HD 6555	5213	BD +22 174	K0III	5.410	28 Dec. 2013	4 x 600	160
HD 10057	7632	BD +1 293	K2III	3.059	30 Dec. 2013	4 x 300	300
HD 29065	21297	HR 1452	K3III	1.820	2 Dec. 2012	4 x 60	120
HD 49520	32844	58 Aur	K3III	2.024	28 Dec. 2013	4 x 90	200
HD 106760	59856	HR 4668	K0.5III	2.110	29 Dec. 2013	4 x 90	300
HD 211683	110141	BD +09 5019	K2	4.612	31 Dec. 2013	4 x 400	205
HD 212074	110382	BD +14 4782	K1IV	5.013	1 Jan. 2014	4 x 600	200
HD 216174	112731	HR 8688	K1III	2.625	30 Dec. 2013	4 x 150	195
HD 233517	...	BD +53 1239	K2	6.637	30 Nov. 2012	4 x 900	160
Thick Disk							
HD 249	607	BD +25 5073	K1IV	4.879	28 Dec. 2013	4 x 600	190
HD 3546	3031	ϵ And	G7III	2.070	28 Dec. 2013	4 x 120	260
HD 9138	7007	μ Psc	K3III	1.660	30 Nov. 2012	4 x 30	210
HD 15596	11698	27 Ari	G8III	3.861	31 Dec. 2013	4 x 400	300
HD 37171	26386	HR 1908	K5III	2.120	28 Dec. 2013	4 x 90	145
HD 44030	30142	BD +25 1223	K4III	4.139	28 Dec. 2013	4 x 300	300
HD 50778	33160	tet CMa	K4III	0.660	30 Nov. 2012	4 x 20	130
HD 71597	41538	BD +0 2305	K1IV	4.503	1 Dec. 2012	4 x 500	190
HD 77729	44592	BD +26 1895	K4III	4.170	30 Dec. 2013	4 x 400	160
HD 96436	54336	65 Leo	K0III	3.329	29 Dec. 2013	4 x 300	240
HD 103813	58306	BD +27 2073	K0III	5.057	28 Dec. 2013	4 x 600	125
HD 105740	59334	BD +17 2445	G9III	5.847	29 Dec. 2013	4 x 600	165
HD 107328	60172	c Vir	K0.5III	2.200	29 Dec. 2013	4 x 90	180
HD 121146	67589	HR 5227	K2IV	3.655	17 Feb. 2014	4 x 300	200
HD 221345	116076	14 And	G8III	2.331	28 Dec. 2013	4 x 120	190
BD +27 2057	G7III	7.220	30 Dec. 2013	4 x 900	100
Halo							
HD 8724	6710	BD +16 149	G5	5.636	31 Dec. 2013	4 x 500	195
HD 63791	38621	BD +62 959	G0	5.427	1 Jan. 2014	4 x 900	300

NOTE—Spectral types and K magnitudes from SIMBAD. Sixteen stars have probabilities greater than 90% of belonging to their predicted population, while seven stars are in the range $0.75 \leq P < 0.9$ (HD 29065, thin; HD 37171, thick; HD 49520, thin; BD +27 2057, thick; HD 6555, thin; HD 106760, thin; and HD 211683, thin), and four stars are in the range $0.5 < P < 0.75$ (HD 10057, thin, at $P=0.52$; HD 50778, thick, at $P=0.56$; HD 3546, thick, at $P=0.64$; and HD 212074, thin, at $P=0.72$). While HD 10057 is designated as a thin-disk member with $P = 0.52$, it was identified as a thick-disk giant with a 97% probability by Pakhomov (2013) based on criteria from Mishenina et al. (2004).

total exposure time, and the signal-to-noise (S/N) ratio of the resulting spectra are provided in Table 1. S/N ratios of the sample star spectra range from 100 to 300, while the S/N ratios of telluric-line stars were in excess of 300. Sample spectra of the sample stars are shown in Figure 1.

3. ANALYSIS

The abundances of fluorine and sodium in the sample stars were determined using spectrum synthesis with the local thermodynamic equilibrium (LTE) spectral analysis code MOOG (V. 2019, Sneden 1973). Synthetic spectra covering the $2.3359 \mu\text{m}$ (1-0) R9 feature of HF and the Na I line at $2.3379 \mu\text{m}$ were convolved with Gaussian profiles to fit the final reduced spectra. Model atmo-

sphere parameters (effective temperature, surface gravity, $[\text{Fe}/\text{H}]$, and microturbulence) were adopted from literature sources identified in Table 2. Model atmospheres were interpolated from the MARCS grid (Gustafsson et al. 2008) and spherical models were used for our sample of giants. Sample best fit syntheses for the HF and Na I line are shown in Figure 2.

Following Ryde et al. (2020), we adopt the meteoritic solar fluorine abundance of $A(F)_{\odot} = 4.42$ from Lodders et al. (2009) due to the large uncertainties of the solar fluorine values derived from modeling umbral spectra.

The molecular line data used for analysis of the 23358.329 \AA (1-0) R9 feature of HF has historically

Table 2. Stellar Parameters and Abundances

Star	T_{eff}	Log g	ξ	[Fe/H]	Ref	log $\epsilon(F)$	[F/Fe]	log $\epsilon(Na)$	[Na/Fe]
	(K)		(km s ⁻¹)						
Thin Disk									
HD 6555	4720	3.00	1.15	-0.09	b	6.40	0.25
HD 10057	4130	1.70	1.35	-0.30	b	4.15	0.03	5.89	-0.05
HD 29065	3990	1.77	2.30	-0.35	c	4.00	-0.07	5.89	0.00
HD 49520	4300	2.35	2.20	0.00	c	4.20	-0.22	6.24	0.00
HD 106760	4510	2.70	2.10	-0.29	c	4.16	0.03	5.95	0.00
HD 211683	4450	1.80	1.35	-0.13	b	4.62	0.33	6.11	0.00
HD 212074	4700	2.55	1.30	+0.05	b	6.39	0.10
HD 216174	4440	2.53	2.40	-0.53	c	5.71	0.00
HD 233517	4475	2.25	1.85	-0.37	p	5.87	0.00
Thick Disk									
Arcturus	4286	1.66	1.74	-0.52	q	3.73	-0.17	5.91	0.19
HD 249	4850	2.96	1.17	-0.15	b	6.29	0.20
HD 3546	5109	2.83	1.73	-0.50	i	5.79	0.05
HD 9138	4395	2.07	1.98	-0.34	a	4.56	0.48	6.25	0.35
HD 15596	4936	3.06	1.19	-0.53	i	5.76	0.05
HD 37171	4000	1.25	1.35	-0.55	b	3.90	0.03	5.74	0.05
HD 44030	4300	1.00	3.00	-0.70	d	4.23	0.51	5.79	0.25
HD 50778	4084	1.70	1.50	-0.22	e	4.13	-0.07
HD 71597	4271	1.90	1.80	-0.40	f	<3.65	<-0.37	5.89	0.05
HD 77729	4270	2.00	3.00	-0.40	d	4.20	0.18
HD 96436	4750	2.75	1.50	-0.50	k	5.94	0.20
HD 103813	4816	3.11	1.01	-0.36	l	6.08	0.20
HD 105740	4700	2.50	1.00	-0.51	m	5.93	0.20
HD 107328	4442	1.95	1.51	-0.39	n	5.85	0.00
HD 121146	4400	2.25	1.90	-0.06	o	4.64	0.28	6.43	0.25
HD 221345	4740	2.61	1.44	-0.27	i	5.97	0.00
BD +27 2057	4810	2.25	1.25	-0.51	g	6.03	0.30
Halo									
HD 8724	4757	1.77	1.65	-1.53	h	4.41	-0.30
HD 63791	4725	1.70	1.60	-1.68	j	4.46	-0.10

NOTE—We use $\log \epsilon(Fe)_{\odot} = 7.50$ from [Asplund et al. \(2009\)](#), $\log \epsilon(F)_{\odot} = 4.42$ from [Lodders et al. \(2009\)](#), and $\log \epsilon(Na)_{\odot} = 6.24$ from [Asplund et al. \(2009\)](#).

References— (a) [Luck & Heiter \(2007\)](#); (b) [Pakhomov \(2013\)](#); (c) [McWilliam \(1990\)](#); (d) [Gratton & Ortolani \(1984\)](#); (e) [da Silva et al. \(2006\)](#); (f) [Barbuy & Erdelyo-Mendes \(1989\)](#); (g) [Afşar et al. \(2012\)](#); (h) [Hayes et al. \(2018\)](#); (i) [da Silva et al. \(2015\)](#); (j) [Burris et al. \(2000\)](#); (k) [Cottrell & Sneden \(1986\)](#); (l) [Deka-Szymankiewicz et al. \(2018\)](#); (m) [Shetrone \(1996\)](#); (n) [Smiljanic et al. \(2016\)](#); (o) [Luck & Challener \(1995\)](#); (p) [Balachandran et al. \(2000\)](#); (q) [Ramírez & Allende Prieto \(2011\)](#).

varied. We adopted the excitation potential $\chi = 0.227$ from [Decin \(2000\)](#), the HITRAN database ([Rothman et al. 2013](#)), and [Jönsson et al. \(2014a\)](#), $\log gf = -3.962$ from [Jönsson et al. \(2014a\)](#), and dissociation energy of 5.869 from [Sauval & Tatum \(1984\)](#). In early abundance determinations the excitation potential of 0.49 eV was used, which results in a higher fluorine abundance of typically 0.36 (see Section 3.2 in [Nault & Pilachowski 2013](#)). [Jönsson et al. \(2014b\)](#) confirmed that the partition functions used with MOOG and the [Decin \(2000\)](#) line data are compatible with their results. Several other $\log gf$ values have been determined, such as -3.971 ([Lucatello et al. 2011](#)) and -3.956 ([Maiorca et al. 2014](#)), which are similar to the adopted value from [Jönsson](#)

[et al. \(2014a\)](#) and would result in an abundance difference of only ~ 0.01 . Some uncertainty remains in the HF molecule’s dissociation energy, which could result in a lower fluorine abundance of ~ 0.04 dex (see Section 4.1.1 in [Guerço et al. 2019](#)).

Atomic line data for the Na I line at 2.3379 μm were adopted from [Pilachowski & Pace \(2015\)](#), who used the atomic and molecular line list generator `linemake` ([Placco et al. 2021](#)), then confirmed by fitting the Na I line in the Infrared Atlas of the Arcturus Spectrum ([Hinkle et al. 1995](#)).

Multiple CO (2–0) and (3–1) vibration-rotation lines are found near the HF and Na features. The neighboring $C^{12}O^{16}$ lines are included in the synthesis calculation

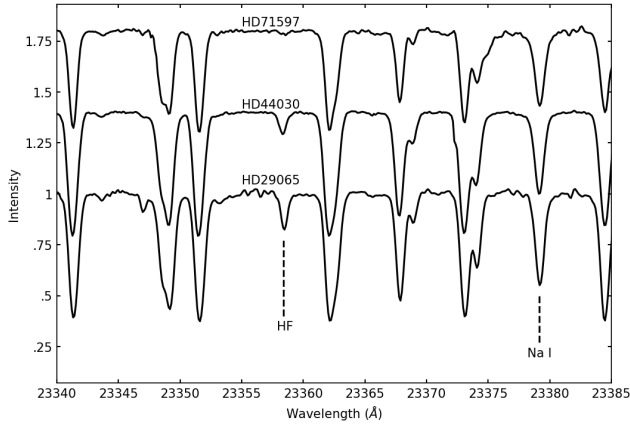


Figure 1. Sample spectra showing the features of HF at 23359 Å and Na I at 23379 Å used in this analysis. The top spectrum is HD 71597, the middle spectrum is HD 44030, and the bottom spectrum is HD 29065. The spectra have been shifted vertically for display purposes. Spectra were selected to show the range of HF equivalent width and signal-to-noise ratio used in the analysis.

using adopted wavelengths, $\log(gf)$ values, and excitation potentials from [Goorvitch \(1994\)](#). Due to the lack of carbon and oxygen abundances for our program stars in the literature, we are unable to measure individual abundances of these elements from only the observed CO lines. The carbon abundance was adjusted to match the observed CO strength, then the abundances of fluorine and sodium were measured in a similar manner.

In one of our program stars (HD 121146), the (2–0) R25 line of $C^{12}O^{17}$ is present and partially blended with the HF line. This $C^{12}O^{17}$ line at 23357.177 Å was included in the synthesis using line data from `linemake`. `linemake` also provided line data for the $C^{12}O^{17}$ line at 23358.237 Å ([Mura-Guzmán et al. 2020](#)), which was not detected in HD 121146.

Final fluorine and sodium abundance measurements are shown in Table 2. We report fluorine abundances for five thin-disk and six thick-disk stars, and one thick-disk star upper limit. Stars must be sufficiently cool (less than ~ 4700 K) to permit the formation of HF in their atmospheres. In our sample stars that are at temperatures above this limit, the HF line was not detected and only measurements of the Na I line were obtained. The $[F/Fe]$ abundance ratios are plotted versus effective temperature in Figure 3, with the metallicity shown in the color bar following [Ryde et al. \(2020\)](#). As observed and discussed in [Pilachowski & Pace \(2015\)](#) and [Ryde et al. \(2020\)](#), we see a rise in fluorine abundance with temperature that is likely a systematic effect. In the warmer stars, the fluorine feature will only be detected if the flu-

orine abundance is high, as the HF feature disappears in warmer stars due to molecular dissociation.

Our analytic methods can be confirmed by measuring the 2.3359 μm (1–0) R9 HF feature in the cool giant standard Arcturus from the atlas of [Hinkle et al. \(1995\)](#). We derived a fluorine abundance of $A(F) = 3.73$ using the atmospheric parameters from [Ramírez & Allende Prieto \(2011\)](#) ($T_{eff} = 4286$ K, $\log g = 1.66$, $[Fe/H] = -0.52$, and $\xi = 1.74$ km s $^{-1}$). This value is comparable with recent Arcturus fluorine measurements by [Guerço et al. \(2019\)](#) ($A(F) = 3.63$), [Abia et al. \(2015\)](#) ($A(F) = 3.78$), [Jönsson et al. \(2014a\)](#) ($A(F) = 3.75$), [Jönsson et al. \(2014b\)](#) ($A(F) = 3.65$ from the 2.3 μm line and $A(F) = 3.73$ from the 12.2 μm line), and [Nault & Pilachowski \(2013\)](#) ($A(F) = 3.75$).

We detect rotation in HD 233517, which is a Li-rich, single K giant known to have a high rotation velocity ($v \sin i$). By fitting the rotational broadening of the 2.3379 μm Na I line, we find a $v \sin i$ of 17.5 ± 4 km s $^{-1}$. The rotational line broadening of HD 233517 was previously measured by [Balachandran et al. \(2000\)](#) and [Strassmeier et al. \(2015\)](#), who report values of 17.6 ± 1.0 km s $^{-1}$ and 17.8 ± 0.1 km s $^{-1}$, respectively.

No known non-LTE (NLTE) corrections exist for the 2.3359 μm (1–0) R9 HF feature. LTE should generally be expected for molecular vibrational-rotational transitions in the ground electronic state ([Hinkle & Lambert 1975](#)). [Li et al. \(2013\)](#) explored the deviations from radiative equilibrium for the 2.3359 μm (1–0) R9 HF line in the low-metallicity range near $[M/H] = -2.0$. They determined that the effects of three-dimensional (3D) model atmospheres on their derived fluorine abundances were insignificant at low gravity and temperature, but larger corrections (> 0.1 dex) were expected at higher gravity and temperature. Our sample consists of stars with temperatures less than 4500 K, with the exception of HD 106760, which has an effective temperature of 4510 K, surface gravity of 2.70, and a derived fluorine abundance of $[F/Fe] = 0.03$. In Figure 3 we detect no dependence of fluorine abundance on effective temperature, providing some assurance that NLTE and 3D effects are not substantial for stars less than ~ 4500 K. With the selection effect of the HF line, where the line is detectable at higher effective temperatures if the abundance is high, it is difficult to identify possible NLTE and 3D effects. However, we can examine the derived abundances at the cool end of our sample, which show no obvious increase in abundance that is indicative of such effects.

No NLTE corrections currently exist for the Na I line at 2.3379 μm . [Cunha et al. \(2015\)](#) discuss NLTE calculations for the studied Na I lines in the APOGEE spectral region in the near-IR H band, finding separ-

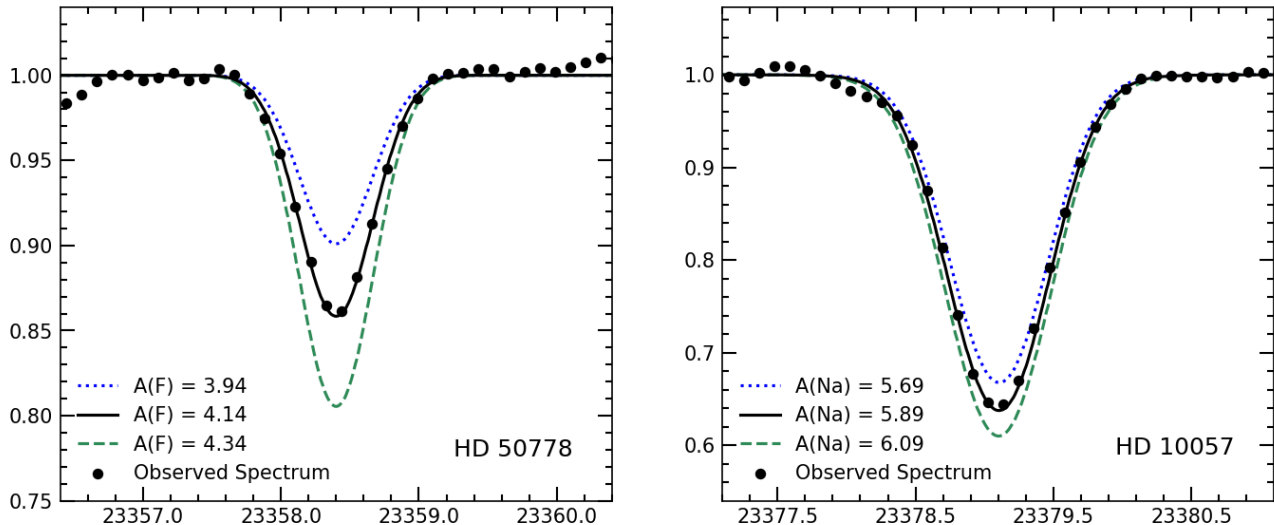


Figure 2. The observed and synthetic spectra for the (1–0) R9 2.3358 μm feature of the HF molecule in HD 50778, and the Na I line at 2.3379 μm in HD 10057. Three syntheses are plotted in each panel, with the best fits being $A(\text{F}) = 4.14$ and $A(\text{Na}) = 5.89$.

tures from LTE to be minimal (≤ 0.04 dex) for their sample of giants in NGC 6791. Our sample of giants has a similar parameter range as Cunha et al. (2015)’s sample, though our metallicities are lower. We observe no temperature trend with derived sodium abundance, as seen in Figure 3.

Uncertainties in our abundance results arise from observational uncertainties and uncertainties in the adopted atmospheric parameters for each star. Observational uncertainties were estimated by altering the smoothing of the synthetic spectrum and the fits themselves until the difference in abundance measurement were distinguishable. To estimate the uncertainties in the adopted stellar atmospheric parameters, the sensitivity of the fluorine abundance to each individual parameter was measured. These uncertainties are summarized in Table 3. Uncertainties may arise from the telluric correction of the near-IR spectra. Fortunately, H_2O only has a few weak lines in the region of interest. The total uncertainty is determined by adding the individual sources in quadrature. Depending on the effective temperature of the star, the total uncertainty for the derived fluorine abundances is less than 0.23 dex across the temperature range from 4000 to 4500 K.

4. COMPARISON TO PREVIOUS WORK

To our knowledge, we present the first fluorine measurements for our sample stars. Figure 4 shows the derived abundances versus metallicity, compared to normal giants from the literature. Fluorine abundances from Li et al. (2013), Jönsson et al. (2014b), Pilachowski

& Pace (2015), Guerço et al. (2019), Ryde et al. (2020), and the data from Jönsson et al. (2017) that Ryde et al. (2020) reanalyzed are included. The measurements from these studies have been scaled to align with the molecular data and solar fluorine abundance used in this study. The derived sodium abundances are also presented in Figure 4, with sodium abundances of red-giant stars in the thin/thick disk and halo from Alves-Brito et al. (2010) for comparison.

Our sample covers a metallicity range from $-0.70 < [\text{Fe}/\text{H}] < 0.00$, with measurements at low- and approximately-solar metallicity. Recent fluorine abundance studies with measurements in this regime include Jönsson et al. (2014b) ($-0.62 < [\text{Fe}/\text{H}] < -0.14$), Pilachowski & Pace (2015) ($-0.6 < [\text{Fe}/\text{H}] < +0.3$), Guerço et al. (2019) ($-1.3 < [\text{Fe}/\text{H}] < 0.00$), and Ryde et al. (2020) ($-1.11 < [\text{Fe}/\text{H}] < +0.37$). For our sample, the average fluorine abundance is $[\text{F}/\text{Fe}] = +0.14 \pm 0.07$ (standard error of the mean, SEM) with a standard deviation of 0.23. The Pilachowski & Pace (2015) sample of ~ 40 normal giants has an average abundance of $[\text{F}/\text{Fe}] = +0.07 \pm 0.04$ (SEM). Average fluorine abundances in Guerço et al. (2019) and Ryde et al. (2020) are $[\text{F}/\text{Fe}] = -0.10 \pm 0.06$ (SEM) and $[\text{F}/\text{Fe}] = +0.03 \pm 0.02$ (SEM), respectively. By taking an average of the fluorine abundances from the 2.3 μm and 12.2 μm where measurements exist from each line, the average fluorine abundance from Jönsson et al. (2014b) is $[\text{F}/\text{Fe}] = -0.09 \pm 0.03$ (SEM).

At approximately-solar metallicity, the abundance measurements from all studies have similar $[\text{F}/\text{Fe}]$ values, though there is an observed scatter (see Figure 4).

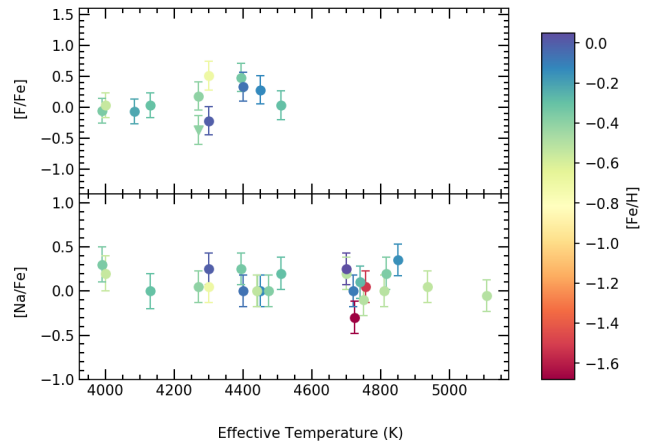
Table 3. Sensitivity to Stellar Parameters

Parameter	log $\epsilon(\text{F})$		log $\epsilon(\text{Na})$	
	$T_{eff}= 4000 \text{ K}$	$T_{eff}= 4500 \text{ K}$	$T_{eff}= 4000 \text{ K}$	$T_{eff}= 4500 \text{ K}$
$\Delta T_{eff} = \pm 100 \text{ K}$	0.18	0.22	0.14	0.12
$\Delta \text{Log } g = \pm 0.3$	0.02	0.00	0.00	0.00
$\Delta \xi = \pm 0.5 \text{ km s}^{-1}$	0.02	0.00	0.12	0.10
$\Delta [\text{Fe}/\text{H}] = \pm 0.1$	0.05	0.03	0.06	0.07
Observational Uncertainty	0.05	0.05	0.05	0.05
Total Uncertainty	0.20	0.23	0.20	0.18

The scatter is greater at solar metallicity than at supersolar metallicities. As seen in Table 3, the dominant source of uncertainty on $[\text{F}/\text{Fe}]$ ratios is from errors in the effective temperature. The methods of determining temperature among different studies may partially explain the observed scatter and differences in average fluorine abundances across different samples. However, fluorine and sodium have similar overall uncertainties due to atmospheric parameters, but the observed scatter in the fluorine abundances is greater than the scatter in the sodium abundances, as seen in Figure 4.

Previously, it has been suggested that fluorine in higher-metallicity stars is dominated by a secondary source (see Section 5.1 in Ryde et al. 2020 for an overview on primary and secondary fluorine production sites and processes). Ryde et al. (2020) found a secondary behavior in their sample stars and concluded that AGB stars are the main channel of formation in the metallicity range of $-0.6 < [\text{Fe}/\text{H}] < 0$. This behavior is demonstrated in the A(F) versus A(Fe I) plot in Figure 4 of Guerço et al. (2022), where the slope indicative of secondary yields is shown to fit the observed trend of fluorine at higher metallicities. Our derived fluorine abundances in the metallicity range of -0.5 to 0.0 are consistent with the values from the literature, following the observed secondary behavior of disk stars.

At lower metallicities, a primary source of fluorine dominates (Guerço et al. 2019; Ryde et al. 2020; Guerço et al. 2022). Guerço et al. (2019) proposes primary behavior at $[\text{Fe}/\text{H}] < -0.5$, and secondary behavior at $[\text{Fe}/\text{H}] > -0.5$. Ryde et al. (2020) suggests at lower metallicities the abundance ratios may decrease more slowly than at higher metallicities, and Ryde et al. (2020) and Guerço et al. (2019) report a near-flat trend of abundance with $[\text{Fe}/\text{H}]$ at low metallicity. Guerço et al. (2019) reports a gradient of $[\text{F}/\text{Fe}]$ for their probable thick-disk/halo stars to have a shallow slope of 0.02 ± 0.03 dex. We report two fluorine measurements in low-metallicity ($[\text{Fe}/\text{H}] < -0.5$ dex) stars. Our two measurements have derived fluorine abundances that are at


Figure 3. Derived abundance vs. effective temperature, with metallicity ($[\text{Fe}/\text{H}]$) indicated by color.

least ~ 0.3 dex greater than the values derived in low-metallicity stars in Guerço et al. (2019) and the upper limits from Ryde et al. (2020). Our abundance determination for HD 44030, which has a $[\text{Fe}/\text{H}] = -0.70$, is comparable to the abundance determinations in the low-metallicity regime for the two metal-poor red giants from Guerço et al. (2019), determined to be probable members of the Monoceros overdensity. The other abundance measurement at low metallicity for the star HD 37171 at $[\text{Fe}/\text{H}] = -0.55$ is comparable to measurements from Pilachowski & Pace (2015) and the data from Jönsson et al. (2017) that Ryde et al. (2020) reanalyzed at a similar metallicity.

5. FLUORINE ENRICHMENT IN THE THIN AND THICK DISKS

Using our classification procedure for kinematic populations detailed in Section 2.1, we assigned the stars from the literature to be members of the thin disk, thick disk, or halo. Gaia DR3 data were utilized when available. In instances where Gaia DR3 data were unavailable, proper motions, parallaxes, and radial velocities came from Gaia DR2 (Gaia Collaboration et al. 2018),

Karataş et al. (2004), Famaey et al. (2005), Gontcharov (2006), van Leeuwen (2007), Massarotti et al. (2008), Famaey et al. (2009), Soubiran et al. (2018), and Jönsson et al. (2020). The final thin-/thick-disk and halo samples from the literature are plotted with our results in Figures 4, 5, and 6. Combining our derived abundances with the values from the literature, we find a final thin-disk fluorine abundance of $[F/Fe] = +0.04 \pm 0.02$ (SEM) with a standard deviation of 0.24, and a thick disk abundance of $[F/Fe] = +0.07 \pm 0.08$ (SEM) with a standard deviation of 0.29. For thin-disk stars in the metallicity range $-0.6 < [Fe/H] < 0.3$, Pilachowski & Pace (2015) find an average $[F/Fe]$ ratio of $+0.07 \pm 0.04$ (SEM), which is comparable to our results. Within the range from approximately $-0.7 < [Fe/H] < 0$, the thin- and thick-disk average abundances do not differ by more than 0.03 dex.

Both our sample and our sample combined with the literature values show a slightly larger dispersion in the thick disk than the thin disk, with standard deviations larger in thick-disk samples. This can be seen in Figures 4 and 5, and is even more pronounced when considering our upper-limit thick-disk measurement for HD 71597. Scatter in $[F/Fe]$ is higher at lower metallicity, which suggests there could be a variation from star to star in the thick disk. The dispersion could be either real or observational as scatter increases as the HF line gets weaker. The $[Na/Fe]$ in Figure 4 shows a relatively flat trend for both the thin and thick disks with the populations overlapping each other, similar to the distribution and pattern observed by Li et al. (2018).

6. CHEMICAL EVOLUTION OF FLUORINE

Finally, we compare the observed fluorine abundances to chemical evolution models to constrain possible nucleosynthetic sources of fluorine. Figure 5 shows our derived fluorine abundances and the kinematically assigned literature sample with recent chemical evolution models fully described in Kobayashi et al. (2011a, 2020), Prantzos et al. (2018), Spitoni et al. (2018), and Grisoni et al. (2020) overlain. As in Figure 4, the literature abundance measurements and theoretical models have been scaled to align with the molecular data and solar fluorine abundance used in this study.

Some models show a peak in $[F/Fe]$ at ~ -0.1 which is explained by different star-formation histories. These histories can lead to different abundance patterns, which can be understood in terms of the time-delay model (Matteucci 2021). The Grisoni et al. (2020) models use a parallel approach (see Grisoni et al. 2017, 2018), where the disks are formed in parallel, but the thick-disk track is shifted to higher metallicities than the thin disk

as a result of its quicker evolution. At solar metallicity, the majority of models show declining $[F/Fe]$ with $[Fe/H]$. The “two-infall” model from Spitoni et al. (2018) matches our derived abundances at low metallicity and solar metallicity quite well. Nonetheless, the data show an increase in $[F/Fe]$ at $\sim +0.25$ which is unexplained by the models. The Grisoni et al. (2020) models have the closest slope to the observed fluorine abundances from the literature at high metallicity.

Thin- and thick-disk stars were distinguished when comparing $[F/O]$ ratios to $[O/H]$ ratios in Grisoni et al. (2020), possibly due to more uncertain yields of Fe. We plot $[F/O]$ vs. $[O/H]$ in Figure 6 using oxygen abundances from Smith & Lambert (1990), Luck & Challener (1995), Meléndez et al. (2008), Hinkel et al. (2014) (Hypatia Catalog), and Jönsson et al. (2020) (APOGEE). We do not see differences between populations, though this may be due to higher uncertainties. At lower metallicities, the thick-disk stars have higher $[F/O]$ measurements than the models.

While sophisticated chemical evolution models of fluorine have been created, the predictions have yet to reproduce all features of the observed abundances. This may in part be due to uncertainties remaining in Galactic chemical evolution models, in addition to the uncertainty in deriving fluorine abundances. Grisoni et al. (2020) point out that the largest uncertainty in Galactic chemical evolution modeling is nucleosynthesis prescriptions, leading to proposed corrections to help explain the observed abundance trends. Many prescriptions may be underestimated: Grisoni et al. (2020) multiplied the yields of AGB stars by 5, Prantzos et al. (2018) proposed a factor of 2 increase in AGB star yields, and Spitoni et al. (2018) increased the yields of AGB stars, novae, and Wolf–Rayet stars. Moreover, there are different nucleosynthesis prescriptions for AGB stars that provide distinctive results when implemented in chemical evolution models. Figure 1 of Grisoni et al. (2020) illustrates how different sets of low- and intermediate-mass star yields result in vastly different fluorine predictions on a plot of $[F/Fe]$ versus $[Fe/H]$. These nucleosynthesis prescriptions affect the model behavior at high metallicity. Instances where the slope of the literature abundances at higher metallicities is not reproduced by a model may be due to the nucleosynthesis prescriptions used for low- and intermediate-mass stars in that model. Further data and investigation into the prescriptions of different nucleosynthetic sources of fluorine are needed to draw definitive conclusions on the origin of fluorine in different stellar populations.

7. SUMMARY

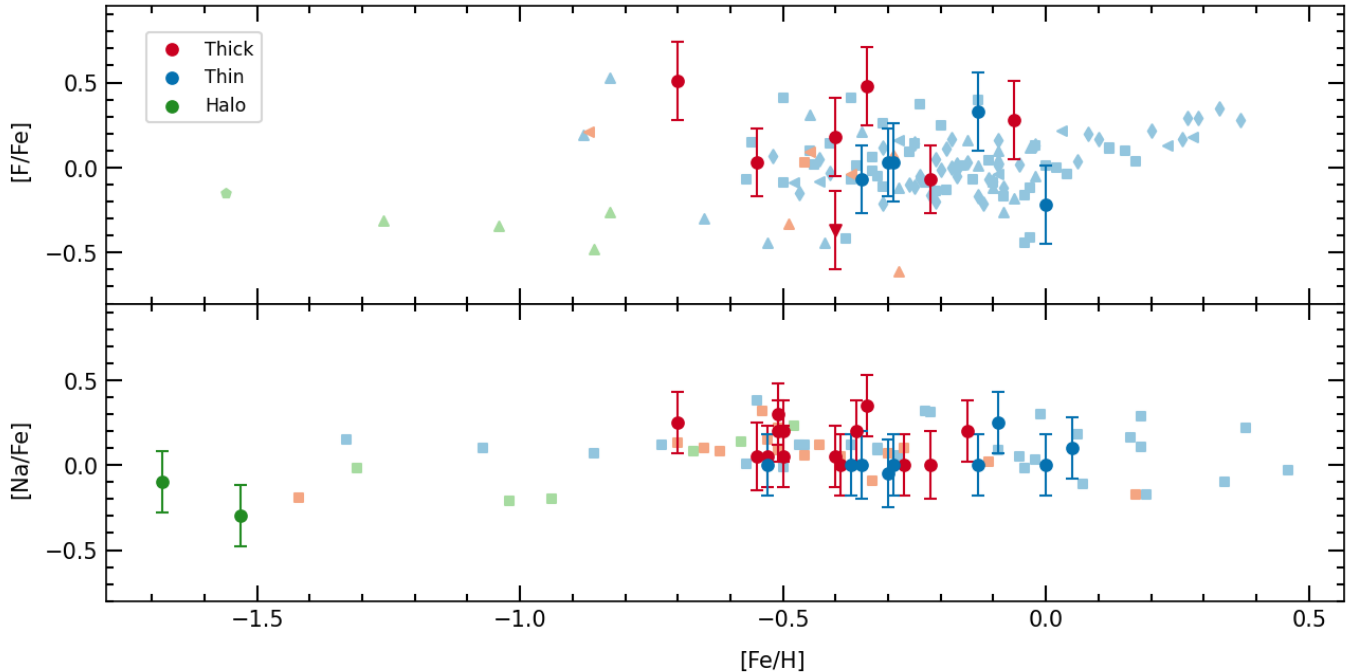


Figure 4. $[F/Fe]$ (upper panel) and $[Na/Fe]$ (lower panel) vs. $[Fe/H]$ for thick disk (red circles), thin disk (blue circles), and halo (green circles) stars. Literature measurements for the thin-disk, thick-disk, and halo populations are shown in light blue, orange, and light green, respectively. Abundances for giants are taken from Li et al. (2013) (pentagons), Jönsson et al. (2014b) (right-pointing arrows), Pilachowski & Pace (2015) (squares), Guerço et al. (2019) (triangles), Ryde et al. (2020) (left-pointing arrows), and the Jönsson et al. (2017) data reanalyzed by Ryde et al. (2020) (diamonds) for $[F/Fe]$ and from Alves-Brito et al. (2010) (squares) for $[Na/Fe]$.

Fluorine and sodium abundances have been determined for a sample of giants in the thin disk, thick disk, and halo. We summarize our findings below.

- Our sample covers a metallicity range from $-0.70 < [Fe/H] < 0.00$. The average fluorine abundance for our sample is $[F/Fe] = +0.14 \pm 0.07$ (SEM) with a standard deviation of 0.23. The derived fluorine abundances are consistent with other studies of fluorine in these populations.
- We report two robust fluorine measurements for stars with $[Fe/H] < 0.5$ dex: $[F/Fe] = +0.51$ (HD 44030) and $[F/Fe] = +0.03$ (HD 37171).
- We identify two stars with high $[F/Fe]$: HD 9138 with $[F/Fe] = +0.48$ and HD 44030 with $[F/Fe] = +0.51$.
- The thin- and thick-disk average $[F/Fe]$ for our sample of stars combined with the literature differ by 0.03 dex.
- There is a larger dispersion in fluorine abundances than sodium abundances despite both species having similar overall uncertainties due to atmospheric parameters, suggesting this dispersion is

real and not observational. The dispersion is slightly larger in the thick disk than the thin.

- Finally, we compare our observations with Galactic chemical evolution models including different nucleosynthesis prescriptions for fluorine. Still, it remains difficult to draw firm conclusions and further data might be needed in this context.

8. ACKNOWLEDGEMENTS

We thank the referee for helpful comments that improved this paper. We are grateful to the Kitt Peak National Observatory and particularly to Karen Butler, Ken Hinkle, Dick Joyce, and Christian Soto for their assistance during the observing runs. We also thank Rashad Givens for his contributions in the early phases of the analysis of the data. C.A.P. acknowledges the generosity of the Kirkwood Research Fund at Indiana University. V.G. acknowledges financial support from INAF under the program “Giovani Astrofisiche ed Astrofisici di Eccellenza - IAF: Astrophysics Fellowships in Italy” (Project: GalacticA, “Galactic Archaeology: reconstructing the history of the Galaxy”). Z.G.M is partially supported by a NASA ROSES-2020 Exoplanet Research Program Grant (20-XRP20 2-0125). This research has made use of the NASA Astrophysics Data System Bib-

liographic Services, the HITRAN database operated by the Center for Astrophysics, and the WEBDA database, operated at the Department of Theoretical Physics and Astrophysics of the Masaryk University. Additionally, this research has made use of the SIMBAD database, operated at CDS, Strasbourg, France. The research shown here acknowledges use of the Hypatia Catalog Database, an online compilation of stellar abundance data as described in Hinkel et al. (2014), which was supported by NASA's Nexus for Exoplanet System Science (NExSS) research coordination network and the Vanderbilt Initiative in Data-Intensive Astrophysics (VIDA). Finally, this work has made use of data from the European Space Agency (ESA) mission *Gaia* ([https://www.](https://www.cosmos.esa.int/gaia)

[cosmos.esa.int/gaia](https://www.cosmos.esa.int/gaia)), processed by the *Gaia* Data Processing and Analysis Consortium (DPAC, <https://www.cosmos.esa.int/web/gaia/dpac/consortium>). Funding for the DPAC has been provided by national institutions, in particular the institutions participating in the *Gaia* Multilateral Agreement.

Facilities: KPNO:2.1m (Phoenix)

Software: IRAF (Tody 1986, 1993), MOOG (Snedden 1973, V. 2019), matplotlib (Hunter 2007), numpy (van der Walt et al. 2011)

REFERENCES

- Abia, C. Recio-Blanco, A., de Laverny, P., Cristallo, S., Domínguez, I., & Straniero, O. 2009, *ApJ*, 694, 971
- Abia, C., Cunha, K., Cristallo, S., de Laverny, P., Domínguez, I., Eriksson, K., Gialanella, L., Hinkle, K., Imbriani, G., Recio-Blanco, A., Smith, V. V., Straniero, O., & Wahlin, R. 2010, *ApJ*, 715, L94
- Abia, C., Cunha, K., Cristallo, S., et al. 2015, *A&A*, 581, A88. doi:10.1051/0004-6361/201526586
- Afşar, M., Sneden, C., & For, B.-Q. 2012, *AJ*, 144, 20
- Alves-Brito, A., Meléndez, J., Asplund, M., et al. 2010, *A&A*, 513, A35. doi:10.1051/0004-6361/200913444
- Asplund, M., Grevesse, N., Sauval, A. J., & Scott, P. 2009, *ARA&A*, 47, 481
- Balachandran, S. C., Fekel, F. C., Henry, G. W., & Uitenbroek, H. 2000, *ApJ*, 542, 978
- Barbuy, B. & Erdelyi-Mendes 1989, *A&A*, 214, 239
- Burris, D. L., Pilachowski, C. A., Armandroff, T. E., et al. 2000, *ApJ*, 544, 302
- Cottrell, P. L. & Sneden, C. 1986, *A&A*, 161, 314
- Cunha, K.; Smith, V. V.; Lambert, et al. 2003, *AJ*, 126, 1305
- Cunha, K., Smith, V. V., Johnson, J. A., et al. 2015, *ApJL*, 798, L41. doi:10.1088/2041-8205/798/2/L41
- da Silva, L., Girardi, L., Pasquini, L., et al. 2006, *A&A*, 458, 609
- da Silva, R., Milone, A. de C., & Rocha-Pinto, H. J. 2015, *A&A*, 580, A24
- Decin, L. 2000, Catholic University of Leuven, Ph.D. Thesis
- Deka-Szymankiewicz, B., Niedzielski, A., Adamczyk, M., et al. 2018, *A&A*, 615, A31
- Ding, P.-J., Zhu, Z., & Liu, J.-C. 2019, *Research in Astronomy and Astrophysics*, 19, 068
- Famaey, B., Jorissen, A., Luri, X., et al. 2005, *A&A*, 430, 165. doi:10.1051/0004-6361:20041272
- Famaey, B., Pourbaix, D., Frankowski, A., et al. 2009, *A&A*, 498, 627. doi:10.1051/0004-6361/200810698
- Gaia Collaboration, Prusti, T., de Bruijne, J. H. J., et al. 2016, *A&A*, 595, A1. doi:10.1051/0004-6361/201833051
- Gaia Collaboration, Brown, A. G. A., Vallenari, A., et al. 2018, *A&A*, 616, A1. doi:10.1051/0004-6361/201833051
- Gaia Collaboration, Vallenari, A., Brown, A. G. A., et al. 2023, *A&A*, 674, A1. doi:10.1051/0004-6361/202243940
- Gontcharov, G. A. 2006, *Astronomy Letters*, 32, 759. doi:10.1134/S1063773706110065
- Goorvitch, D. 1994, *ApJS*, 95, 535.
- Gratton, R. G. & Ortolani, S. 1984, *A&A*, 137, 6
- Grisoni, V., Spitoni, E., Matteucci, F., et al. 2017, *MNRAS*, 472, 3637. doi:10.1093/mnras/stx2201
- Grisoni, V., Spitoni, E., & Matteucci, F. 2018, *MNRAS*, 481, 2570. doi:10.1093/mnras/sty2444
- Grisoni, V., Romano, D., Spitoni, E., et al. 2020, *MNRAS*, 498, 1252. doi:10.1093/mnras/staa2316
- Guerço, R., Cunha, K., Smith, V. V., et al. 2019, *ApJ*, 885, 139. doi:10.3847/1538-4357/ab45f1
- Guerço, R., Ramírez, S., Cunha, K., et al. 2022, *ApJ*, 929, 24. doi:10.3847/1538-4357/ac5c55
- Gustafsson B., Edvardsson B., Eriksson K., et al. 2008, *A&A*486, 951.
- Hall, D. N. B. & Noyes, R. W. 1969, *ApJL*, 4, 13
- Hayes, C. R., Majewski, S. R., Shetrone, M., et al. 2018, *ApJ*, 852, 49
- Hinkle, K. H. & Lambert, D. L. 1975, *MNRAS*, 170, 447. doi:10.1093/mnras/170.3.447
- Hinkle, K., Wallace, L., & Livingston, W. E. (ed.) 1995, *Infrared Atlas of the Arcturus Spectrum, 0.9-5.3 microns* (San Francisco, CA: ASP)

- Hinkel, N. R., Timmes, F. X., Young, P. A., et al. 2014, *AJ*, 148, 54. doi:10.1088/0004-6256/148/3/54
- Hunter, J. D. 2007, *Computing in Science and Engineering*, 9, 90. doi:10.1109/MCSE.2007.55
- Johnson, D. R. H., & Soderblom, D. R. 1987, *AJ*, 93, 864
- Jönsson, H., Ryde, N., Harper, G. M., et al. 2014, *A&A*, 564, A122. doi:10.1051/0004-6361/201423597
- Jönsson, H., Ryde, N., Harper, G. M., et al. 2014, *ApJL*, 789, L41. doi:10.1088/2041-8205/789/2/L41
- Jönsson, H., Ryde, N., Spitoni, E., et al. 2017, *ApJ*, 835, 50. doi:10.3847/1538-4357/835/1/50
- Jönsson, H., Holtzman, J. A., Allende Prieto, C., et al. 2020, *AJ*, 160, 120. doi:10.3847/1538-3881/aba592
- Jorissen, A.; Smith, V. V.; & Lambert, D. L. 1992, *A&A*, 261, 164
- Karataş, Y., Bilir, S., Eker, Z., et al. 2004, *MNRAS*, 349, 1069. doi:10.1111/j.1365-2966.2004.07588.x
- Kobayashi, C., Izutani, N., Karakas, A. I., et al. 2011, *ApJL*, 739, L57
- Kobayashi, C., Karakas, A. I., & Lugaro, M. 2020, *ApJ*, 900, 179. doi:10.3847/1538-4357/abae65
- Li, H. N., Ludwig, H.-G., Caffau, E., et al. 2013, *ApJ*, 765, 51
- Li, C., Zhao, G., Zhai, M., et al. 2018, *ApJ*, 860, 53. doi:10.3847/1538-4357/aac50f
- Lodders, K., Palme, H., & Gail, H.-P. 2009, *LanB*, 4B, 712. doi:10.1007/978-3-540-88055-4_34
- Lucatello, S.; Masseron, T.; Johnson, J. A.; Pignatari, M.; Herwig, F. 2011, *ApJL*, 729, 40
- Luck, R. E. & Challenor, S. L. 1995, *AJ*, 110, 2968. doi:10.1086/117741
- Luck, R. E. & Heiter, U. 2007, *AJ*, 133, 2464
- Maiorca, E., Uitenbroek, H., Uttenthaler, S., et al. 2014, *ApJ*, 788, 149. doi:10.1088/0004-637X/788/2/149
- Massarotti, A., Latham, D. W., Stefanik, R. P., et al. 2008, *AJ*, 135, 209. doi:10.1088/0004-6256/135/1/209
- Matteucci, F. 2021, *A&A Rv*, 29, 5. doi:10.1007/s00159-021-00133-8
- McWilliam, A. 1990, *ApJS*, 74, 1075
- Meléndez, J., Asplund, M., Alves-Brito, A., et al. 2008, *A&A*, 484, L21. doi:10.1051/0004-6361/200809398
- Meynet, G. & Arnould, M. 2000, *A&A*, 355, 176
- Mishenina, T. V.; Soubiran, C.; Kovtyukh, V. V. 2004, *A&A*, 418, 551
- Mura-Guzmán, A., Yong, D., Abate, C., et al. 2020, *MNRAS*, 498, 3549. doi:10.1093/mnras/staa2610
- Nault, K. A. & Pilachowski, C. A. 2012, *AJ*, 146, 153
- Nomoto, K.; Kobayashi, C., & Tominaga, N. 2013, *ARA&A*, 51, 457
- Olive, K. A. & Vangioni, E. 2019, *MNRAS*, 490, 4307. doi:10.1093/mnras/stz2893
- Pakhomov, Yu. V. 2013, *Astronomy Letters*, 39, 54
- Pilachowski, C. A. & Pace, C. 2015, *AJ*, 150, 66. doi:10.1088/0004-6256/150/3/66
- Placco, V. M., Sneden, C., Roederer, I. U., et al. 2021, *Research Notes of the American Astronomical Society*, 5, 92. doi:10.3847/2515-5172/abf651
- Prantzos, N., Abia, C., Limongi, M., et al. 2018, *MNRAS*, 476, 3432. doi:10.1093/mnras/sty316
- Prugniel, Ph., Vauglin, P., & Koleva, M. 2011, *A&A*, 531, A165
- Ramírez, I. & Allende Prieto, C. 2011, *ApJ*, 743, 135. doi:10.1088/0004-637X/743/2/135
- Ramírez, I., Allende Prieto, C., & Lambert, D. L. 2013, *ApJ*, 764, 78. doi:10.1088/0004-637X/764/1/78
- Rothman, L. S., Gorden I. E., Babikov, Y., et al. 2012, *JQSRT*, 130, 4
- Ryde, N., Jönsson, H., Mace, G., et al. 2020, *ApJ*, 893, 37. doi:10.3847/1538-4357/ab7eb1
- Sauval, A. J. & Tatum, J. B. 1984, *ApJS*, 56, 193. doi:10.1086/190980
- Schuler, S. C., Cuhna, K., Smith, V. V., et al. 2007, *ApJ*, 667, 81
- Shetrone, M. D. 1996, *AJ*, 112, 1517
- Smiljanic, R., Romano, D., Bragaglia, A., et al. 2016, *A&A*, 589, A115
- Smith, V. V. & Lambert, D. L. 1990, *ApJS*, 72, 387. doi:10.1086/191421
- Sneden, C. 1973, *ApJ*, 184, 839
- Soubiran, C., Jasniewicz, G., Chemin, L., et al. 2018, *A&A*, 616, A7. doi:10.1051/0004-6361/201832795
- Spitoni, E., Matteucci, F., Jönsson, H., et al. 2018, *A&A*, 612, A16. doi:10.1051/0004-6361/201732092
- Strassmeier, K. G., Carroll, T. A., Weber, M., et al. 2015, *A&A*, 574, A31. doi:10.1051/0004-6361/201424130
- Tody, D. 1986, *Proc. SPIE*, 627, 733. doi:10.1117/12.968154
- Tody, D. 1993, *Astronomical Data Analysis Software and Systems II*, 52, 173
- van der Walt, S., Colbert, S. C., & Varoquaux, G. 2011, *Computing in Science and Engineering*, 13, 22. doi:10.1109/MCSE.2011.37
- van Leeuwen, F. 2007, *A&A*, 474, 653. doi:10.1051/0004-6361:20078357
- Wallace, L., Hinkle, K., & Livingston, W. C. 2001, *NSO Technical Report #01-001*; Tucson: National Solar Observatory
- Womack, K. A., Vincenzo, F., Gibson, B. K., et al. 2023, *MNRAS*, 518, 1543. doi:10.1093/mnras/stac3180

Woosley, S. E. & Haxton, W. C. 1988, *Nature*, 334, 45.
doi:10.1038/334045a0

Wu, Y., Singh, H. P., Prugniel, P., Gupta, R., & Kolea, M.
2011, *A&A*, 525, 71

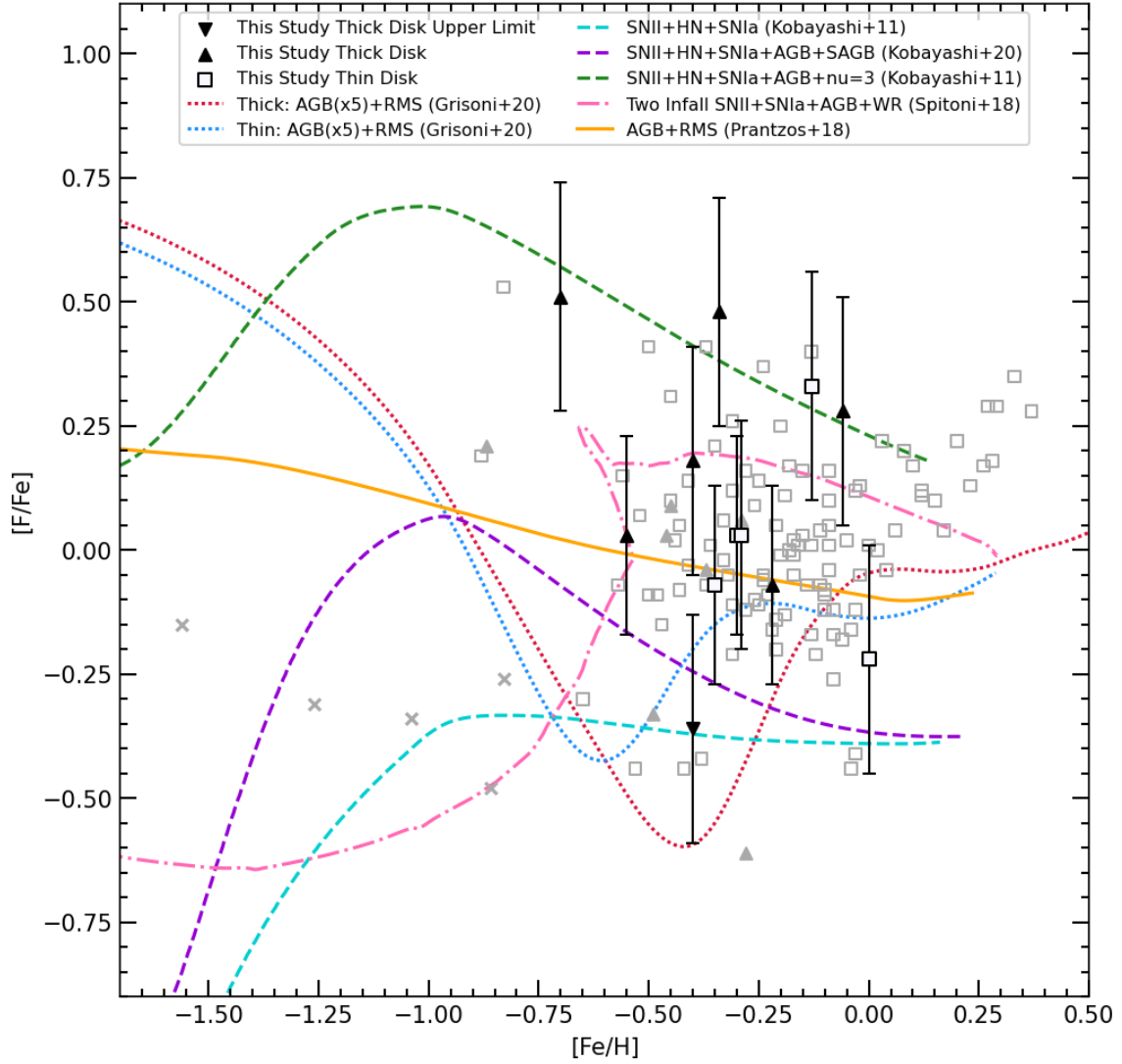


Figure 5. $[F/Fe]$ vs. $[Fe/H]$ for our sample of thin- and thick-disk stars with measurements from the literature. Chemical evolution models from the literature are shown for different combinations of production channels. Literature measurements from Li et al. (2013), Pilachowski & Pace (2015), Guergo et al. (2019), and Ryde et al. (2020) are shown in gray. Thin-disk stars are indicated with open squares, thick-disk stars with filled triangles, and halo stars with crosses.

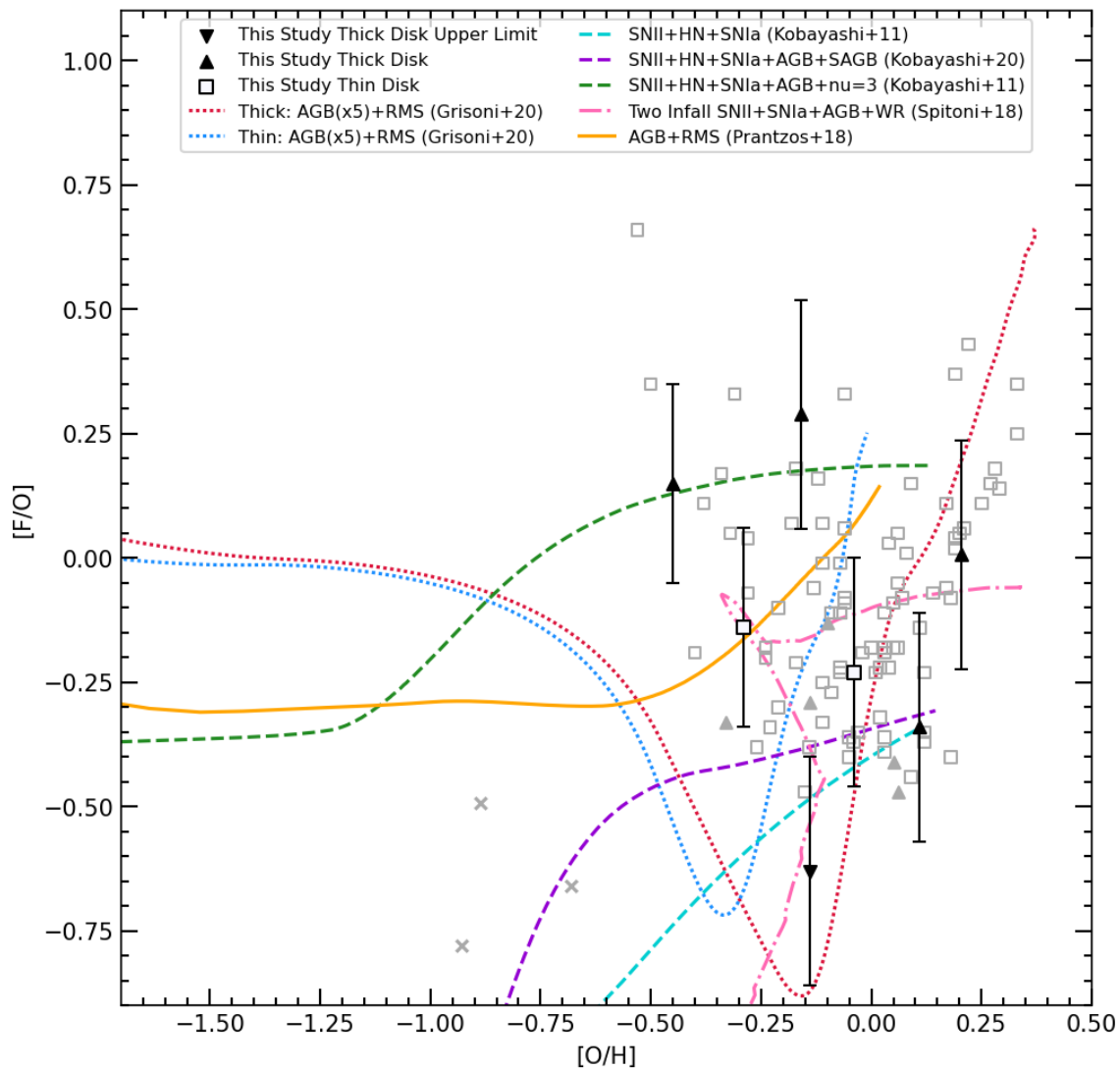


Figure 6. $[F/O]$ vs. $[O/H]$ for our sample of thin- and thick-disk stars with measurements from the literature. Symbols are as defined in Figure 5.